Chemical Science

ROYAL SOCIETY OF CHEMISTRY

EDGE ARTICLE

View Article Online
View Journal | View Issue

Cite this: *Chem. Sci.*, 2023, **14**, 8615

All publication charges for this article have been paid for by the Royal Society of Chemistry

Exploiting reduced-symmetry ligands with pyridyl and imidazole donors to construct a second-generation stimuli-responsive heterobimetallic $[PdPtL_4]^{4+}$ cage†

Aston C. Pearcy, [a] Lynn S. Lisboa, [a] Dan Preston, [b] Nick B. Page,[a] Tristan Lawrence,[a] L. James Wright, [c] Christian G. Hartinger [c] and James D. Crowley *[a]

A new sequential metalation strategy that enables the assembly of a new more robust reduced symmetry heterobimetallic $[PdPtL_4]^{4+}$ cage **C** is reported. By exploiting a low-symmetry ditopic ligand (**L**) that features imidazole and pyridine donor units we were able to selectively form a $[Pt(L)_4]^{2+}$ "open-cage" complex. When this was treated with Pd(II) ions the cage **C** assembled. ^{1}H and DOSY nuclear magnetic resonance (NMR) spectroscopy and electrospray ionisation mass spectrometry (ESIMS) data were consistent with the quantitative formation of the cage and the heterobimetallic structure was confirmed by single crystal X-ray crystallography. The cage **C** was shown to bind anionic guest molecules. NMR studies suggested that these guests interacted with the cavity of the cage in a specific orientation and this was confirmed for the mesylate ion (MsO^-) : **C** host–guest adduct using X-ray crystallography. In addition, the system was shown to be stimulus-responsive and could be opened and closed on demand when treated with appropriate stimuli. If a guest molecule was bound within the cage, the opening and closing was accompanied by the release and re-uptake of the guest molecule.

Received 14th March 2023
Accepted 13th July 2023

DOI: 10.1039/d3sc01354e

rsc.li/chemical-science

Introduction

High symmetry is generally a desirable property often associated with beauty. Many self-assembled architectures in Nature display high-symmetry (*i.e.* viral protein capsids, ferritin, and protein tetramers such as haemoglobin).[1,2] Inspired by these systems, much of the early work in self-assembled metallosupramolecular architectures (MSAs) targeted highly symmetric assemblies.[3–13] There are now many approaches that enable the straightforward generation of these high-symmetry metallo-architectures from simple building blocks. The resulting materials have been exploited for a range of applications, including encapsulation,[14–16] separations,[17] catalysis,[18–21] environmental remediation,[22] and biological activity.[23,24]

While these are important applications and the results are impressive they almost universally exploit the cavities of the MSAs in a dissimilar way to active sites in enzymes. Unlike the cavities of these high-symmetry MSAs, enzyme active sites tend to be lower symmetry and this provides the basis for their high substrate selectivity. As such, there has been a recent move toward developing lower symmetry MSAs in an effort to further enhance the properties and applications of these materials. There have been three main approaches to reduced/lower symmetry MSAs, these are (1) combine a metal ion with two or more different ligands and selectively form hetero-ligated MSAs, (2) combine a metal ion and a lower symmetry ligand to selectively form a single MSA, or (3) generate heterometallic MSAs.[25–29]

M_2L_4 lantern-shaped cages (Fig. 1a)[30–35] have been at the forefront of efforts to generate reduced symmetry MSAs from lower symmetry ligands. This is due to their relative simplicity, as they only contain four ligands and two metal ions. A range of heteroleptic $[M_2La_xLb_y]$ cages (where $x = 3$ or 2 and $y = 1$ or 2) have been developed exploiting geometric, steric, templating or supramolecular effects to provide selectivity.[36–43] These approaches have also been extended to larger heteroleptic palladium(II) architectures.[44–46] In addition to these heteroleptic systems, a series of reduced symmetry homoleptic $[Pd_2L_4]^{4+}$, $[Pd_4L_8]^{8+}$ and $[Pd_6L_{12}]^{12+}$ cages have been synthesised using lower symmetry ligands.[47–54] Reduced/lower symmetry MSAs have also been generated using a heterometallic approach.[26] However, often the ligands used to generate heterometallic MSAs are bi- or tri-dentate

[a]*Department of Chemistry, University of Otago, PO Box 56, Dunedin 9054, New Zealand. E-mail: jcrowley@chemistry.otago.ac.nz*

[b]*Research School of Chemistry, Australian National University, Canberra, ACT 0200, Australia*

[c]*School of Chemical Sciences, University of Auckland, Private Bag 92019, Auckland 1142, New Zealand*

† Electronic supplementary information (ESI) available. CCDC 2175042–2175046. For ESI and crystallographic data in CIF or other electronic format see DOI: https://doi.org/10.1039/d3sc01354e

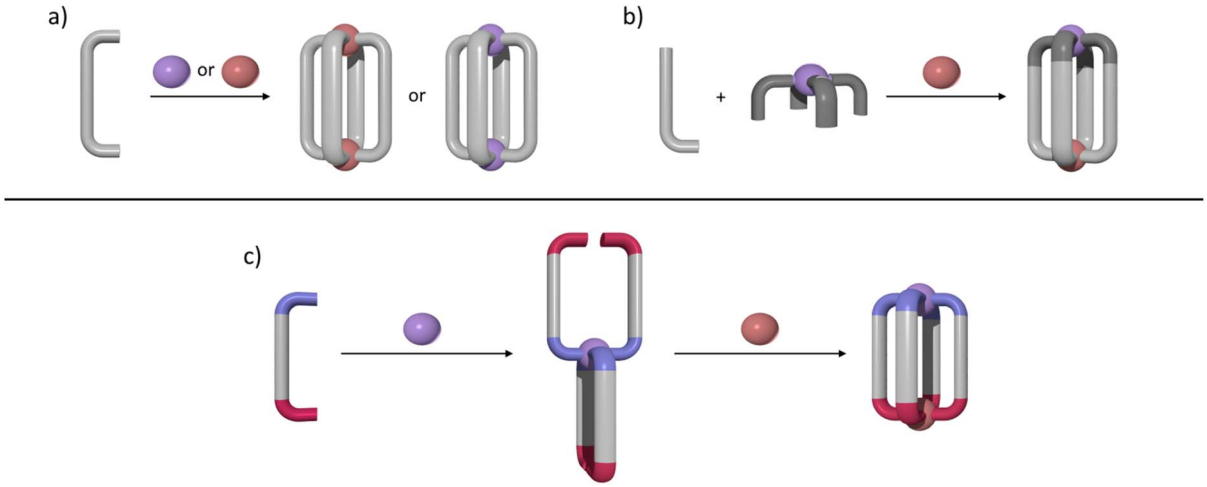

Fig. 1 Cartoon representations of: (a) synthesis of homometallic high symmetry $[M_2L_4]^{4+}$ cages where M = Pd^{II} or Pt^{II}; (b) synthesis of a low-symmetry heterobimetallic $[PdPtL_4]^{4+}$ cage using the subcomponent self-assembly approach; (c) formation of a heterobimetallic $[PdPtL_4]^{4+}$ cage from a low-symmetry ditopic ligand *via* a sequential complexation strategy. Colours: Pd^{II} brick, Pt^{II} purple, bis-monodentate ligands light or dark grey. Periwinkle blue or red ligand caps denote differing donor units.

donor systems in conjunction with a mono-dentate donor unit and exploit the chelate effect to provide metal ion selectivity.[55,56] Generating $[M^1M^2L_4]$-type heterometallic architectures that feature ditopic linker ligands with two monodentate donor units has proven to be much more difficult.

We have recently synthesised the first example of a low-symmetry heterobimetallic $[PdPtL_4]^{4+}$ cage.[57] However, our approach used the subcomponent self-assembly method from a pre-formed inert platinum(II) tetrapyridylaldehyde complex, a substituted pyridylamine building block and a labile palladium(II) complex (Fig. 1b). The reversible formation of the dynamic covalent imine and labile palladium(II)–pyridyl bonds enabled the quantitative formation of the heterobimetallic $[PdPtL_4]^{4+}$ cage. While this method provides access to $[PdPtL_4]^{4+}$ architectures and has been exploited to generate related heterometallic double cavity cages,[58] the presence of the water-labile imine functionality limits the potential applications of these systems. Herein, we report a new method for synthesis of more robust $[PdPtL_4]^{4+}$ architectures (Fig. 1c). Using a low-symmetry ditopic ligand that features imidazole and pyridine as two monodentate coordinating units with markedly different donor strengths, the platinum(II) and palladium(II) ions of the target $[PdPtL_4]^{4+}$ heterobimetallic cage can be introduced sequentially (Fig. 1c). As with our previously reported $[PdPtL_4]^{4+}$ cage, this architecture is stimuli-responsive and can be opened and closed reversibly with concurrent guest release and binding.[59,60] Importantly, we also show that, unlike other low-symmetry assemblies, the new low-symmetry cage can bind anionic guests in a specific orientation, in a manner reminiscent of biologically occurring molecular containers such as enzymes.

Results and discussion

For the sequential complexation strategy (Fig. 1c) to be successful, we required a low-symmetry ditopic ligand that contained two monodentate coordinating units with different donor strengths. Due to the difference in pK_a between imidazole (6.95)[61] and pyridine (5.20)[62] we reasoned that a ligand featuring those donor units might be appropriate. However, before committing to that ligand design we carried out some competition experiments with palladium(II) ions and 1-methylimidazole (**meim**) and 3-[1-(phenylmethyl)-1*H*-1,2,3-triazol-4-yl]pyridine (**3-pytri**)[63] (ESI, Sections 1 and 2†). Combining $[Pd(CH_3CN)_4](BF_4)_2$, **meim** and **3-pytri** in a 1 : 4 : 4 ratio in CD_3CN led to the quantitative formation of $[Pd(\mathbf{meim})_4](BF_4)_2$. Similarly, reacting the preformed $[Pd(\mathbf{3\text{-}pytri})_4](BF_4)_2$ complex with **meim** (4 eq.) led to the instantaneous displacement of the **3-pytri** ligands and quantitative formation of the $[Pd(\mathbf{meim})_4](BF_4)_2$ complex (ESI, Section 2, Fig. S21 and S22†). This strongly suggested that a ditopic ligand containing both imidazole pyridine donors would be a suitable candidate for selective, sequential heterodimetalation. As such we targeted the synthesis of **L** (Scheme 1 and ESI, Section 1, Scheme S1†).

The synthesis of low-symmetry ligand **L** began with the desymmetrisation of commercially available α,α′-dibromo-*p*-xylene (ESI, Scheme S1†). α,α′-Dibromo-*p*-xylene (1 eq.) and NaN_3 (1 eq.) were heated at 60 °C in acetonitrile for 24 h to give 1-(azidomethyl)-4-(bromomethyl)benzene[64,65] in modest yields (isolated yields ranged from 27–45%). This mono-substituted intermediate (1 eq.) was then stirred with imidazole (1.1 eq.) and KOH (2 eq.) for 4 h at room temperature (RT) in acetonitrile to give 1-(4-(azidomethyl)benzyl)-1*H*-imidazole in good yield (77%). This azide building block (1 eq.) was then treated with 3-ethylnylpyridine (1.63 eq.) using standard copper-catalysed azide–alkyne cycloaddition (CuAAC) "click" conditions ($CuSO_4 \cdot 5H_2O$ (0.68 eq.) and sodium ascorbate (0.9 eq.) in 4 : 1 DMF : H_2O at RT for 24 h) providing the low-symmetry ditopic imidazole pyridine ligand **L** in excellent yield (91%). **L** was characterised using ^1H, ^{13}C and DOSY nuclear magnetic resonance (NMR) spectroscopies, electrospray ionisation mass spectrometry (ESIMS) and the molecular structure was

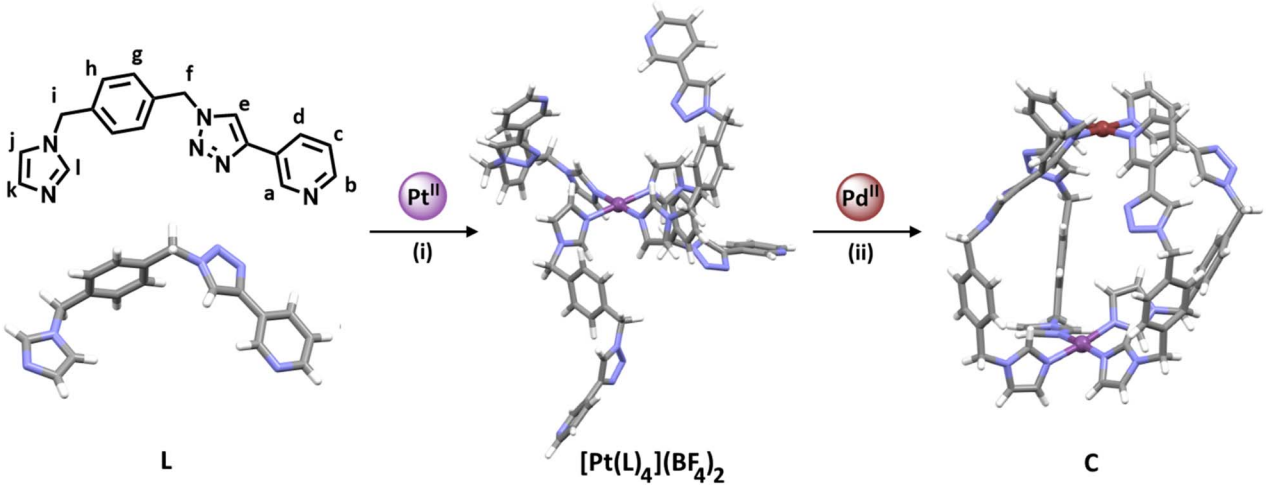

Scheme 1 Synthesis of the platinum(II) complex $[Pt(\mathbf{L})_4](BF_4)_2$, and the heterobimetallic low-symmetry cage (**C**): (i) **L** (4.1 eq.), $AgBF_4$ (2.2 eq.), and $[Pt(DMSO)_2Cl_2]$ (1 eq.), d_6-DMSO, 60 °C, 7 days. (ii) $[Pt(\mathbf{L})_4](BF_4)_2$ (1 eq.), $[Pd(CH_3CN)_4](BF_4)_2$ (1 eq.), CD_3CN, RT, 10 min ([**L**] = 21.1 mM, $[[Pt(\mathbf{L})_4](BF_4)_2]$ = 5.27 mM). The stick model (MMFF) of $[Pt(\mathbf{L})_4](BF_4)_2$ was generated using SPARTAN'18.[66] Stick models of **L** and **C** are the molecular structures determined by X-ray diffraction analysis. Colours: Pd^{II} brick, Pt^{II} purple, N periwinkle blue, C grey, H white. Solvent molecules and counterions omitted for clarity.

determined using X-ray crystallography (Scheme 1 and ESI, Section 1, Fig. S31†).

With the low-symmetry ditopic ligand **L** in hand, we attempted to selectively form the platinum(II) complex $[Pt(\mathbf{L})_4](BF_4)_2$ in which each ditopic ligand is coordinated to platinum through the imidazole nitrogen donor only. **L** (4.1 eq.), $AgBF_4$ (2.2 eq.), and $[Pt(DMSO)_2Cl_2]$ (1 eq.) were combined in d_6-DMSO at 60 °C in the absence of light and the reaction monitored using ^{1}H NMR spectroscopy and ESIMS (ESI, Fig. S8–S10 and S22–S24†). After one day the resonances due to free ligand **L** had vanished and were replaced by two sets of shifted signals (ESI, Fig. S22 and S23†).

ESIMS data showed the presence of a major peak at m/z = 730.2721, which was consistent with the molecular formula $[Pt(\mathbf{L})_4]^{2+}$, suggesting the mono-Pt^{II} complex had formed. With continued heat over seven days the ratio of the two sets of signals slowly changed to a point where a 85 : 15 ratio[67] was obtained.[68] Addition of ethyl acetate to this mixture led to the precipitation of pure $[Pt(\mathbf{L})_4](BF_4)_2$ in good isolated yield (68%). ESIMS of the isolated material in CH_3CN again displayed a major peak at m/z = 730.2721 with a second smaller peak at m/z = 1546.5385 consistent with the formation of $[Pt(\mathbf{L})_4]^{2+}$ and $[Pt(\mathbf{L})_4](BF_4)^+$ ions. The observed isotope patterns matched those calculated for the 2+ and 1+ ions, respectively (ESI, Fig. S10†). Comparison of the ^{1}H NMR spectrum of the ligand **L** with the spectrum of the isolated colourless material showed that the chemical shifts of the pyridyl ($H_{a–d}$) and triazole (H_e) resonances remained essentially unchanged upon coordination to Pt^{II}, whereas the imidazole resonances ($H_{j,k\ and\ l}$) all moved significantly upon complex formation. This was consistent with the formation of a linkage isomer where all ligands are coordinated to the Pt^{II} ion *via* the imidazole donor units (Fig. 2 and ESI, Fig. S8†). Additionally, the ^{1}H DOSY NMR spectra (CD_3CN, 298 K) of **L** and $[Pt(\mathbf{L})_4](BF_4)_2$ showed that all the proton resonances within the individual samples had the same diffusion coefficients ($D_{\mathbf{L}} = 12.0 \times 10^{-10}$ m^2 s^{-1} and $D_{[Pt(\mathbf{L})_4](BF_4)_2} = 5.15 \times 10^{-10}$ m^2 s^{-1}), suggesting formation of a single product (ESI, Section 4, Fig. S24–S30, Table S1†). The platinum(II) complex diffused more slowly than **L** consistent with the formation of a larger structure. While we have been unable to confirm the molecular structure *via* X-ray crystallography, the combined data suggest that the tetraimidazole linkage isomer of $[Pt(\mathbf{L})_4](BF_4)_2$ (MMFF molecular model, Fig. 1) was formed.

The isolated complex $[Pt(\mathbf{L})_4](BF_4)_2$ (1 eq.) was then combined with $[Pd(CH_3CN)_4](BF_4)_2$ (1 eq.) in either CD_3CN or d_6-DMSO at room temperature and the reaction was monitored *via* ^{1}H NMR spectroscopy. Within 10 minutes, signals due to the free pyridyl unit ($H_{a–d}$) had completely vanished and were replaced by a new set of resonances shifted downfield ($\Delta\delta$ = 0.20–0.25 ppm, d_6-DMSO, Fig. 2b and c). Large downfield shifts of the α-pyridyl protons (H_a and H_b) were observed, characteristic of coordination of the palladium(II) ion. Resonances due to platinum(II) coordinated imidazole units remained relatively unchanged (Fig. 2b and c). The new set of ^{1}H NMR signals is distinct from those of both **L** and $[Pt(\mathbf{L})_4](BF_4)_2$. The ^{1}H DOSY NMR spectrum of the reaction mixture revealed that all the new resonances possess the same diffusion coefficient, suggesting the clean formation of a single product. The diffusion coefficient ($D_{\mathbf{C}} = 5.54 \times 10^{-10}$ m^2 s^{-1}) of the cage is different from that of the ligand **L** ($D_{\mathbf{L}} = 12.0 \times 10^{-10}$ m^2 s^{-1}) and similar to that of $[Pt(\mathbf{L})_4](BF_4)_2$ ($D_{[Pt(\mathbf{L})_4](BF_4)_2} = 5.15 \times 10^{-10}$ m^2 s^{-1}), consistent with the formation of a larger cage architecture. ESIMS data obtained from the reaction mixture also supported the formation of the $[PdPt(\mathbf{L})_4](BF_4)_4$ heterobimetallic cage, **C**. The major peak at m/z = 391.6139 was consistent with the molecular formula $[PdPt(\mathbf{L})_4]^{4+}$ and the observed isotope pattern matched that calculated for this 4+ ion.

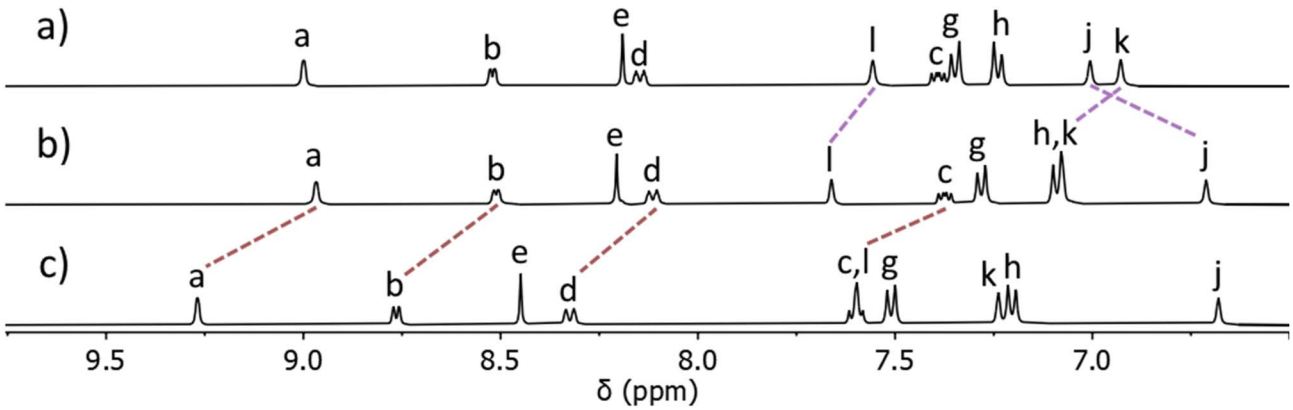

Fig. 2 Stacked partial ^{1}H NMR spectra (400 MHz, d_6-DMSO, 298 K) of (a) ligand **L**, (b) the $[Pt(\mathbf{L})_4](BF_4)_2$ complex, and (c) heterobimetallic cage **C** ([**L**] = 21.1 mM). Proton labels correspond to those shown in Fig. 1 and the ESI.†

Other smaller peaks at m/z = 551.1534 and 870.2332, consistent with the $[PdPt(\mathbf{L})_4(BF_4)]^{3+}$ and $[PdPt(\mathbf{L})_4(BF_4)_2]^{2+}$ ions, respectively, were also observed (ESI, Fig. S13†). The heterometallic low-symmetry cage **C** was isolated as a pale-yellow solid in 87% yield from acetonitrile solution by addition of excess ice-cold diethyl ether. The solid was dissolved in nitromethane and diethyl ether was vapour-diffused into the solution to provide colourless crystals of a suitable quality for single-crystal X-ray diffraction analysis. This unequivocally confirmed the formation of the heterobimetallic low-symmetry $[PdPt(\mathbf{L})_4]^{4+}$ cage (Fig. 3 and ESI, Section 5, Fig. S32†). The two metal ions are bridged by four ligands **L** adopting a *syn* arrangement. As indicated by the ^{1}H NMR analysis, the platinum(II) ion is coordinated by the four imidazole units of the low-symmetry ligand and the palladium(II) ion is coordinated to the four pyridyl units. The nitrogen atoms of the 1,2,3-triazole moieties are not coordinated to either metal ion. The Pd···Pt distance (10.449 Å) is slightly smaller than that of the related imine-based heterobimetallic cage,[57] and comparable to similar, more rigid dipyridyl homometallic cages,[69–73] and other low-symmetry assemblies.[74–76] The cavity of the cage **C** contains a molecule of nitromethane and a BF_4^- anion. Hydrogen bonding is observed between both the guest molecules with a variety of different units on the cage. The nitromethane molecule interacts with three of the four inwardly pointing imidazole protons. The BF_4^- ion interacts with all four α-pyridyl protons (as is often observed in related heterometallic cages) two inwardly pointing triazole protons, and one of the inwardly pointing imidazole protons (Fig. 3 and ESI, Section 5, Fig. S32†).

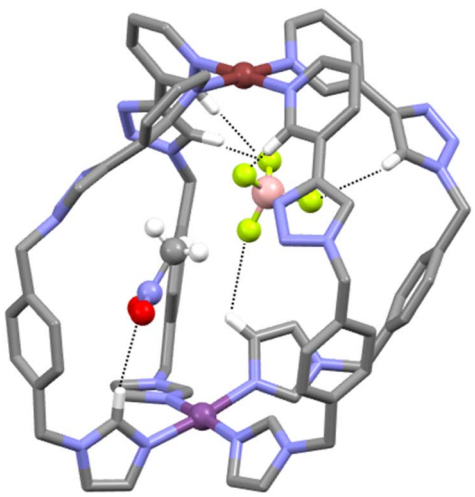

Fig. 3 Molecular structure of the heterobimetallic low-symmetry $[PdPt(\mathbf{L})_4]^{4+}$ cage **C**. A BF_4^- anion and a CH_3NO_2 molecule occupy the cavity of **C**. Colours: Pd^{II} brick, Pt^{II} purple, N periwinkle blue, C grey, H white, B pick, F green. Hydrogen atoms involved in H-bonding interactions (···) are shown. All other hydrogen atoms, most solvents of crystallisation and counterions have been omitted for clarity.

Having successfully generated the second low-symmetry heterobimetallic $[PdPt(\mathbf{L})_4]^{4+}$ cage (**C**), we then examined if the architecture was a thermodynamic or kinetically metastable product. The cage **C** was initially heated in CD_3CN solution at either 50 °C or 75 °C and the solution speciation was monitored using ^{1}H NMR spectroscopy (ESI, Section 6, Fig. S35 and S36†). The ^{1}H NMR spectra of **C** were unchanged after 4 days of heating in CD_3CN (at either 50 or 75 °C) indicating that the dimetallic complex is robust under these conditions. Similar experiments were then carried out using d_6-DMSO as the solvent. The cage **C** was unchanged after four days at 50 °C in d_6-DMSO (Fig. S37†). When **C** was heated at 75 °C or 100 °C in d_6-DMSO changes were observed (Fig. S38†). After 24 hours at 75 °C a new species can be observed. However, even after 4 days at that temperature in d_6-DMSO, **C** remains the major (>90%) species present (Fig. S38†). At 100 °C in d_6-DMSO the rearrangement/isomerisation process is faster. After 24 hours at 100 °C **C** is still the major (50%) compound in solution but several other species can be observed. As the solution is heated further the speciation continues to change and after 4 days only a small amount (10–15%) of **C** remains. The other species observed are presumed to be different $[PdPt(\mathbf{L})_4]^{4+}$ cage isomers. The combined results suggest that **C** is a kinetically metastable architecture. However, the complex is kinetically robust in both CD_3CN and d_6-DMSO over a range of temperatures.

The molecular structure of the low-symmetry heterometallic cage **C** confirmed that the cavity of the cage was accessible for guest molecules (Fig. 3). Therefore, we investigated the host–guest (HG) chemistry of the system with a wide variety of neutral organic and inorganic guest molecules (ESI, Fig. S41†). The HG interactions were examined using ^{1}H NMR spectroscopy and ESIMS. In a series of experiments, one of the potential guest molecules (2 eq.) was combined with cage **C** (1 eq.) in CD_3CN at 298 K and the ^{1}H NMR spectrum acquired (ESI, Section 7, Fig. S42–S44†). The ^{1}H NMR spectrum of the host–guest mixture was compared to the spectra of the "free" host and guest compounds (ESI, Fig. S42 and S43†). Disappointingly, no complexation-induced shifts (CIS) were observed for either the host or the guest resonances, suggesting that none of these neutral guests interacted with the cavity of cage **C**. Consistent with the ^{1}H NMR spectra, the ESIMS data displayed no peaks due to HG complexes. Molecular models (SPARTAN'18,[66] MMFF, see ESI, Section 7, Fig. S40†) suggest that there are no obvious steric interactions that would prevent host–guest formation for the majority of the HG pairs examined. The lack of neutral guest binding appears to be caused primarily by the BF_4^- counter-anions, outcompeting the neutral guests and preferentially occupying the cage cavity (Fig. 3 and ESI, Fig. S39†). This competitive anion binding behaviour has been observed before in related homometallic cages.[77]

Due to the lack of binding observed with neutral molecules, we turned to anionic sulfonate, organotrifluoroborate and phosphate ester guest molecules as these have been well established to bind within related homometallic cage systems.[78–86] We examined methanesulfonate (**MsO**$^-$), *p*-toluenesulfonate (**TsO**$^-$), tolyltrifluoroborate (**tolBF$_3$**$^-$) and dimethylphosphate (**dimephos**$^-$). All four of the anions displayed CIS consistent with guest binding (ESI, Section 7†). For example, upon titration of **MsO**$^-$ into an CD_3CN solution of **C**, a large CIS of the H_a proton ($\Delta\delta = 0.55$, with 2 eq. of **MsO**$^-$) was observed (Fig. 4 and ESI, Fig. S50†). ESIMS data of the HG mixture also provided evidence for the formation of a **C**⊂**MsO**$^-$ host–guest adduct, and indicated a 1 : 1 **C** : **MsO**$^-$ ratio, with large peaks at m/z = 553.8112 ($[\mathbf{C}\subset\mathbf{MsO}^-]^{3+}$) and m/z = 874.2178 ($[\mathbf{C}\subset\mathbf{MsO}^-(BF_4^-)]^{2+}$) (Fig. 4 and ESI, Fig. S49†). Similar NMR and ESIMS data was obtained from CD_3CN mixtures of **C** and **TsO**$^-$ (ESI, Fig. S45–S48†). Disappointingly, mixtures of **C** and either **tolBF$_3$**$^-$ or **dimephos**$^-$ did not display any peaks due the HG adducts in the ESIMS data potentially suggesting that the HG interaction with those guests is weaker than those found with the sulfonates.

The interactions of anionic guest molecules with cage **C** were examined further using ^{1}H NMR spectroscopic titrations (CD_3CN, 298 K) and the data was curve-fitted using bindfit[87–89] to obtain the association constants (*K*, ESI, Section 7, Table S5†). Consistent with the ESIMS data, both sulfonate systems provided an excellent fit to a 1 : 1 binding model ($K_{\mathbf{MsO}^-} = 29\,400 \pm 2700$ M^{-1} and $K_{\mathbf{TsO}^-} = 17\,200 \pm 1600$ M^{-1}). The smaller, more basic **MsO**$^-$ has a slightly stronger interaction with the cage **C** compared to the larger, less basic **TsO**$^-$. The titration data with the **tolBF$_3$**$^-$ guest also provided an excellent fit to a 1 : 1 binding model and the interaction was weaker ($K_{\mathbf{tolBF3}^-} = 2190 \pm 40$ M^{-1}) than what had been found with the sulfonates. Interestingly, the NMR titration data from the interaction of **C** with **dimephos**$^-$ was consistent with a 1 : 2 HG interaction ($K_{1(\mathbf{dimephos}^-)} = 5870 \pm 320$ M^{-1}, $K_{2(\mathbf{dimephos}^-)} = 1540 \pm 70$ M^{-1}, ESI, Fig. S54–S57, Table S5†).

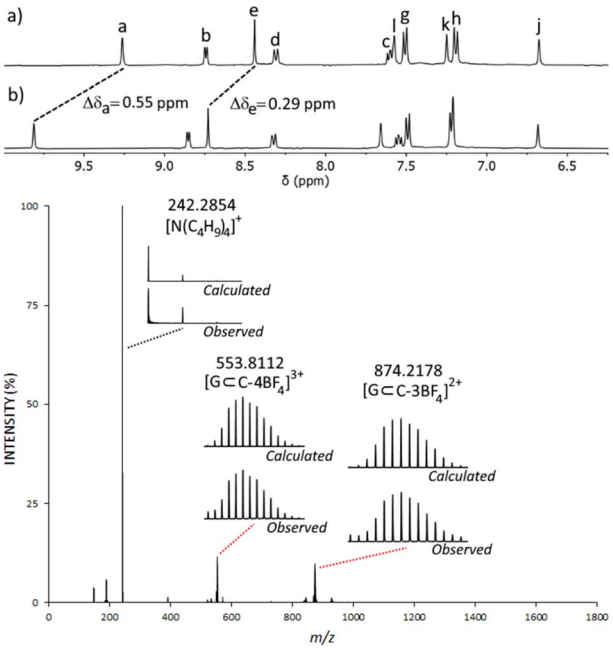

Fig. 4 Top: stacked partial ^{1}H NMR spectra (400 MHz, [D_3]acetonitrile, 298 K) of (a) **C** and (b), **C** + **MsO**$^-$ (2 eq.) ([**C**] = 0.150 mM). Bottom: ESI-mass spectrum obtained from an acetonitrile solution of **C** (1 eq.) and **MsO**$^-$ (2 eq.). G refers to the **MsO**$^-$ guest molecule.

The lower symmetry of cage **C** means that there are potentially two different binding modes for the anionic guest: one where the anions bind at the $[Pd(py)_4]^{2+}$ end of the cage and the other where the guests interact with the $[Pt(im)_4]^{2+}$ end (ESI, Fig. S61†). The largest CIS observed in the ^{1}H NMR data obtained from HG mixtures with the sulfonate and organotrifluoroborate anions were for the pyridyl (H_a) and triazole (H_e) protons of **C** (Fig. 4 and ESI, Section 7†). Little to no shifts were observed for the imidazole ($H_{j,k,l}$) resonances of **C**. The data for the **C** : **dimephos**$^-$ 1 : 2 HG complex was similar, large CIS were observed for the pyridyl (H_a) and triazole (H_e) protons of **C** at lower equivalents (0–3 eq.) of **dimephos**$^-$. As more equivalents (5–42) of **dimephos**$^-$ are added to the mixture the H_a and H_e resonances stop shifting and the imidazole resonances (H_l and H_j) begin to move (ESI, Fig. S54†). The CIS data observed for the 1 : 1 HG complexes strongly suggest that the anions all interact selectively with the $[Pd(py)_4]^{2+}$ end of the cage as has been observed in related homometallic cages.[78–82] The CIS data obtained for the 1 : 2 HG complex formed with **dimephos**$^-$ is also consistent with the first guest binding selectively at the $[Pd(py)_4]^{2+}$ end of the cage while the second anion then interacts with the $[Pt(im)_4]^{2+}$ end of **C**. Additional support for this HG orientation was obtained from X-ray crystallography (Fig. 5 and ESI, Section 7, Fig. S53†). Vapor diffusion of diethyl ether into an acetonitrile solution of the cage **C** and **MsO**$^-$ (2 eq.) provided

colourless crystals suitable for single-crystal X-ray diffraction analysis. Determination of the molecular structure unequivocally confirmed the formation of the HG complex **C⊂MsO**$^-$ (Fig. 5 and ESI, Fig. S53†). The Pd–Pt distance (10.086 Å) in the HG complexes is slightly smaller than that of the parent cage (10.449 Å, *vide infra*). Importantly, the structure revealed that the **MsO**$^-$ guest molecule is interacting, through hydrogen bonding, with the $[Pd(py)_4]^{2+}$ motif of the heterometallic cage, consistent with the NMR data. The **MsO**$^-$ guest is rotationally disordered, but clearly forms hydrogen bonds to the endohedral α-pyridyl protons of the $[Pd(py)_4]^{2+}$ unit. The C···OS distances ranged from 3.12 to 3.26 Å, and the C–H···OS distances from 2.33 to 2.37 Å. Similar interactions have been observed in a range of related homometallic dipalladium cages.[78–82,90,91] There are also interactions with the triazole protons consistent with the CIS observed in solution. We note that the BF_4^- counter anion in the X-ray structure of the "free" **C** (Fig. 3) is also interacting with the $[Pd(py)_4]^{2+}$ end of the cage providing additional solid-state support for the host–guest selectivity.

Having established that **C** can act as a host for anionic guest molecules, we next examined the stimulus responsiveness of the architecture. We and others have shown that addition of the base *N*,*N*′-dimethylaminopyridine (DMAP) to a Pd^{II} architecture can remove the labile palladium(II) ions as the complex $[Pd(DMAP)_4]^{2+}$, and release free ligand.[57,69,92] We have also shown that addition of DMAP to a Pd^{II}/Pt^{II} heterobimetallic architecture preferentially removes the more labile palladium(II) metal ion, leaving the coordination environment of the relatively inert platinum(II) metal ion untouched.[57] This process is completely reversible and the addition of acid preferentially protonates the DMAP ligands, leading to reformation of the cage architecture. As we have used DMAP and *p*-toluenesulfonic acid (TsOH) as external stimuli previously, we chose to employ them in this new heterobimetallic system to examine if the cage could be reversibly opened and closed (ESI, Section 8, Scheme S2, Fig. S62–S65†).

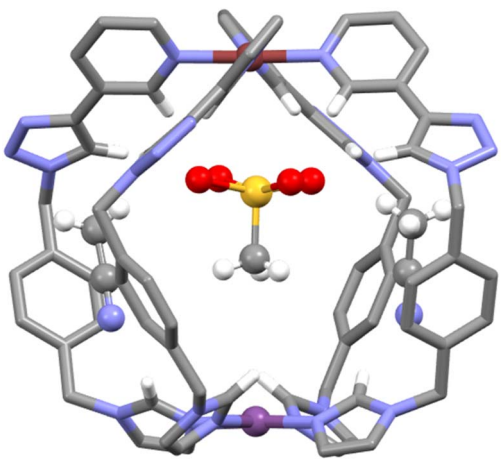

Fig. 5 Molecular structure of the **C⊂MsO**$^-$ host–guest adduct. The **MsO**$^-$ guest is rotationally disordered. Colours: Pd^{II} brick, Pt^{II} purple, N periwinkle blue, C grey, H white, O red, S orange. Hydrogen atoms involved in H-bonding interactions are shown. All other hydrogen atoms, most solvents of crystallisation and counterions have been omitted for clarity.

DMAP (1–5 eq.) was titrated into a d_6-DMSO solution of **C** and the reaction monitored *via* ^{1}H NMR spectroscopy (Fig. S64†). Signals attributable to **C** decreased in intensity, while a new set of signals that matched those of $[Pt(\mathbf{L})_4](BF_4)_2$ grew in intensity after each addition of DMAP. Another set of signals due to a $[Pd(DMAP)_4]^{2+}$ complex also increased in intensity as more equivalents of DMAP were added. These observations indicate the successful opening of the cage. After 4 equivalents of DMAP had been added, the addition of one more equivalent of DMAP did not result in any further changes to the chemical shifts of the complex, and no signals were observed for free **L**. This suggests that an excess of DMAP under the conditions of this experiment was insufficient to extract the inert platinum(II) ion from the imidazole pocket of the $[Pt(\mathbf{L})_4](BF_4)_2$ complex.

TsOH (5 eq.) was then added to the resulting $[Pt(\mathbf{L})_4](BF_4)_2$: $[Pd(DMAP)_4]^{2+}$: DMAP mixture, and the reaction monitored *via* ^{1}H NMR spectroscopy (Fig. S64†). Resonances due to the $[Pt(\mathbf{L})_4](BF_4)_2$ open complex steadily decreased in intensity, while a new set of signals that matched those of **C** grew in intensity after each addition of TsOH. Two more sets of resonances also steadily grew in intensity over the course of the experiment, assigned as protonated DMAP and deprotonated TsOH. These results are consistent with the reformation of **C**. Similar results are obtained when using methanesulfonic acid (MsOH) in the place of TsOH.

Having confirmed that **C** can open and close on demand, we then examined if this ability persists in the presence of a guest (Fig. 6 and ESI, Fig. S66 and S67†). The **C⊂MsO**$^-$ host–guest adduct (Fig. 6a) was formed by addition of **MsO**$^-$ (1 eq.) to a CD_3CN solution of **C** (1 eq.). As detailed before large CIS are observed for H_a and H_e of the cage confirming the formation of the HG complex, additionally the methyl resonance of the bound **MsO**$^-$ anion (H_{Me} = 2.01 ppm) is shifted upfield from "free" **MsO**$^-$ (H_{Me} = 2.41 ppm, ESI, Fig. S66†). DMAP (4 eq.) was then added to the **C⊂MsO**$^-$ host–guest mixture and the reaction monitored using ^{1}H NMR spectroscopy (Fig. 6b). Much like with "free" **C**, when DMAP was added to the HG complex the palladium(II) ions are removed from the cage and the $[Pd(DMAP)_4]^{2+}$ and $[Pt(\mathbf{L})_4]^{2+}$ complexes are formed (Fig. 6b). This was accompanied by release of the **MsO**$^-$ guest (H_{MeO} = 2.43 ppm). Upon addition of methanesulfonic acid (MsOH, 4 eq.) to this mixture, reformation of **C** was observed along with protonation of the DMAP ligands (Fig. 6c). The reformation of **C** occurs with reuptake of **MsO**$^-$ guest molecules, with large CIS observed for H_a and H_e. The ^{1}H NMR spectrum of the reformed host–guest adduct (Fig. 6c) is similar, but not exactly identical, to that of the original **C⊂MsO**$^-$ host–guest complex (Fig. 6a). This is because the solution now contains 5 equivalents of **MsO**$^-$ after the deprotonation of MsOH, which further shifts the resonances (H_a and H_e) of the host–guest adduct. Using TsOH in place of MsOH also provides similar results when switching the host–guest adduct open and closed, but the final HG spectrum (after the switching has been completed) is more

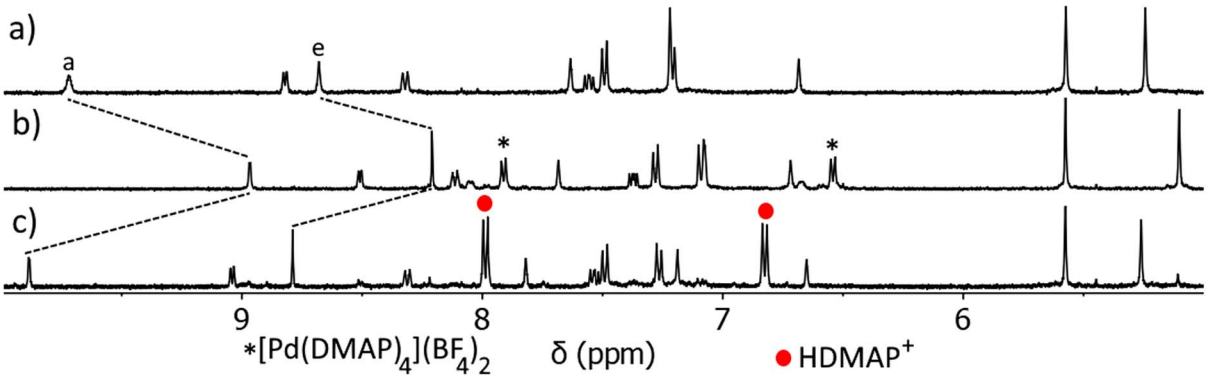

Fig. 6 Stacked partial ^{1}H NMR spectra (400 MHz, CD_3CN, 298 K) of (a) **C**⊂**MsO**$^-$ at a 1 : 1 ratio ([**C**] = 1.00 mM), (b) $[Pt(\mathbf{L})_4](BF_4)_2$ open complex after the addition of DMAP (4 eq.), (c) restored **C**⊂**MsO**$^-$ host–guest adduct after addition of MsOH (4.1 eq.).

complicated due to competition between **MsO**$^-$ (1 eq.) and **TsO**$^-$ (4 eq.) for the cavity of **C** (ESI, Fig. S67†).

The results described above show that **C** retains all the key properties of the 1st generation imine-based heterobimetallic $[PdPt(\mathbf{L})_4]^{4+}$ cage.[57] While this imine-based cage was stable in polar aprotic solvents (acetonitrile, nitromethane and DMSO) when it was exposed to water (5 or 50% in DMSO) the imines hydrolysed and the cage decomposed.[93,94] To examine if the second generation heterobimetallic $[PdPt(\mathbf{L})_4]^{4+}$ cage **C** was more robust in aqueous conditions we carried out two stability experiments using ^{1}H NMR spectroscopy (ESI, Fig. S68 and S69†). Initially, **C** was dissolved in a 19 : 1 d_6-DMSO : D_2O mixture and monitored over 21 days. There was no sign of any cage decomposition. A similar experiment in a 1 : 1 d_6-DMSO : D_2O mixture was then carried out. Again, no decomposition of the cage **C** was observed. These experiments indicate that the 2nd generation heterobimetallic $[PdPt(\mathbf{L})_4]^{4+}$ cage **C** is considerably more robust in aqueous conditions when compared to the parent imine-based cage.

Conclusions

We have developed a method that enables the formation of the low-symmetry heterobimetallic $[PdPtL_4]^{4+}$ cage **C**. By synthesising a low-symmetry ligand that features coordinating units of sufficiently different donor strengths, the individual donor units can be selectively coordinated to different metal ions in a stepwise fashion. This strategy enabled the formation of the complex $[Pt(\mathbf{L})_4](BF_4)_2$, which can be transformed through the addition of palladium(II) ions to the heterobimetallic $[PdPtL_4]^{4+}$ cage in quantitative yield. Formation of the cage was examined with ^{1}H and DOSY NMR spectroscopies as well as ESIMS, and unequivocally confirmed using X-ray crystallography. The cage was shown not bind any of the neutral guest molecules screened in the solvents used. However, the cage was able to strongly encapsulate a range of different anions (**MsO**$^-$, **TsO**$^-$, **tolBF$_3$**$^-$ and **dimephos**$^-$). Most importantly, solution NMR data and solid-state X-ray data from the host–guest complexes indicated that the anions interact orientationally selectively with the $[Pd(py)_4]^{2+}$ end of the cage **C**.

Much like the first generation, imine-based $[PdPtL_4]^{4+}$ cage, **C** was shown to be stimuli-responsive. Upon addition of DMAP the cage was opened through the formation of the complexes $[Pd(DMAP)_4]^{2+}$, and it could be closed again by addition of MsOH or TsOH which protonated the DMAP ligands and released free palladium(II) ions back into the system resulting in spontaneous reformation of **C**. This same process could also be carried out on the **C**⊂**MsO**$^-$ host–guest adduct. In this case the guest molecule was released on deactivation of host–guest interactions when the cage was converted to the open platinum(II) complex. Reuptake of the guest molecule was then observed when the cage was reformed on addition of acid to release free Pd^{II} ions.

While the current cage **C** has limited guest binding capabilities, its stability in aqueous conditions suggests that more water soluble analogues should be able to take advantage of the hydrophobic effect and bind a wider range of neutral guest molecules.[3] These new systems should provide access to switchable enzyme-like catalysts.[71,95–99]

Data availability

The data that support the findings of this study are available in the ESI† of this article. All experimental procedures, characterisation and titration data are available in the ESI.† Crystallographic data for the structures reported herein have been deposited as CCDC 2175042–2175046.

Author contributions

AP, JC, CH, and LW conceived the idea. JC, CH, and LW obtained the funding. AP and JC analysed the data and wrote the manuscript. AP conducted the synthesis, host–guest chemistry and crystallography. TL carried out the model studies. NP assisted the ligand synthesis. LL assisted the collection of host–guest and crystallographic data. DP collected and analysed the DOSY NMR data. All authors provided feedback on the manuscript drafts and approved the submission.

Conflicts of interest

There are no conflicts to declare.

Acknowledgements

ACP thanks the University of Otago and the John Edmond Trust for MSc scholarships. LSL thanks the University of Otago for a PhD scholarship. JDC thanks the University of Otago, Department of Chemistry and the MacDiarmid Institute for Advanced Materials and Nanotechnology for funding. All authors are grateful to the Marsden Fund for supporting this work through a grant (UOA1726).

Notes and references

1 D. L. Caulder and K. N. Raymond, *J. Chem. Soc., Dalton Trans.*, 1999, 1185–1200.
2 D. L. Caulder and K. N. Raymond, *Acc. Chem. Res.*, 1999, **32**, 975–982.
3 E. G. Percastegui, T. K. Ronson and J. R. Nitschke, *Chem. Rev.*, 2020, **120**, 13480–13544.
4 D. Zhang, T. K. Ronson and J. R. Nitschke, *Acc. Chem. Res.*, 2018, **51**, 2423–2436.
5 N. B. Debata, D. Tripathy and H. S. Sahoo, *Coord. Chem. Rev.*, 2019, **387**, 273–298.
6 S. Saha, I. Regeni and G. H. Clever, *Coord. Chem. Rev.*, 2018, **374**, 1–14.
7 H. D. Mai, N. M. Tran and H. Yoo, *Coord. Chem. Rev.*, 2019, **387**, 180–198.
8 S. Chakraborty and G. R. Newkome, *Chem. Soc. Rev.*, 2018, **47**, 3991–4016.
9 H. Wang, Y. Li, N. Li, A. Filosa and X. Li, *Nat. Rev. Mater.*, 2021, **6**, 145–167.
10 T. R. Cook and P. J. Stang, *Chem. Rev.*, 2015, **115**, 7001–7045.
11 M. D. Ward, *Chem. Commun.*, 2009, 4487–4499.
12 K. Harris, D. Fujita and M. Fujita, *Chem. Commun.*, 2013, **49**, 6703–6712.
13 A. J. McConnell, *Chem. Soc. Rev.*, 2022, **51**, 2957–2971.
14 M. Yoshizawa, J. K. Klosterman and M. Fujita, *Angew. Chem., Int. Ed.*, 2009, **48**, 3418–3438.
15 L. Catti, R. Sumida and M. Yoshizawa, *Coord. Chem. Rev.*, 2022, **460**, 214460.
16 M. Yoshizawa and M. Yamashina, *Chem. Lett.*, 2017, **46**, 163–171.
17 D. Zhang, T. K. Ronson, Y.-Q. Zou and J. R. Nitschke, *Nat. Rev. Chem.*, 2021, **5**, 168–182.
18 M. Morimoto, S. M. Bierschenk, K. T. Xia, R. G. Bergman, K. N. Raymond and F. D. Toste, *Nat. Catal.*, 2020, **3**, 969–984.
19 C. M. Hong, R. G. Bergman, K. N. Raymond and F. D. Toste, *Acc. Chem. Res.*, 2018, **51**, 2447–2455.
20 M. D. Ward, C. A. Hunter and N. H. Williams, *Acc. Chem. Res.*, 2018, **51**, 2073–2082.
21 R. J. Hooley, *Synlett*, 2020, **31**, 1448–1463.
22 E. G. Percastegui, *Chem. Commun.*, 2022, **58**, 5055–5071.
23 H. Sepehrpour, W. Fu, Y. Sun and P. J. Stang, *J. Am. Chem. Soc.*, 2019, **141**, 14005–14020.
24 A. Pöthig and A. Casini, *Theranostics*, 2019, **9**, 3150–3169.
25 S. Pullen, J. Tessarolo and G. H. Clever, *Chem. Sci.*, 2021, **12**, 7269–7293.
26 M. Hardy and A. Lützen, *Chem.–Eur. J.*, 2020, **26**, 13332–13346.
27 J. Lewis and J. Crowley, *ChemPlusChem*, 2020, **85**, 815–827.
28 D. Tripathy, N. B. Debata, K. C. Naik and H. S. Sahoo, *Coord. Chem. Rev.*, 2022, **456**, 214396.
29 C. T. McTernan, J. A. Davies and J. R. Nitschke, *Chem. Rev.*, 2022, **122**, 10393–10437.
30 D. A. McMorran and P. J. Steel, *Angew. Chem., Int. Ed.*, 1998, **37**, 3295–3297.
31 A. Schmidt, A. Casini and F. E. Kühn, *Coord. Chem. Rev.*, 2014, **275**, 19–36.
32 M. Han, D. M. Engelhard and G. H. Clever, *Chem. Soc. Rev.*, 2014, **43**, 1848–1860.
33 D. Bardhan and D. K. Chand, *Chem.–Eur. J.*, 2019, **25**, 12241–12269.
34 N. B. Debata, D. Tripathy and D. K. Chand, *Coord. Chem. Rev.*, 2012, **256**, 1831–1945.
35 G. H. Clever and P. Punt, *Acc. Chem. Res.*, 2017, **50**, 2233–2243.
36 A. M. Johnson and R. J. Hooley, *Inorg. Chem.*, 2011, **50**, 4671–4673.
37 M. Yamashina, T. Yuki, Y. Sei, M. Akita and M. Yoshizawa, *Chem.–Eur. J.*, 2015, **21**, 4200–4204.
38 D. Preston, J. E. Barnsley, K. C. Gordon and J. D. Crowley, *J. Am. Chem. Soc.*, 2016, **138**, 10578–10585.
39 R. Zhu, W. M. Bloch, J. J. Holstein, S. Mandal, L. V. Schäfer and G. H. Clever, *Chem.–Eur. J.*, 2018, **24**, 12976–12982.
40 W. M. Bloch, J. J. Holstein, W. Hiller and G. H. Clever, *Angew. Chem., Int. Ed.*, 2017, **56**, 8285–8289.
41 W. M. Bloch, Y. Abe, J. J. Holstein, C. M. Wandtke, B. Dittrich and G. H. Clever, *J. Am. Chem. Soc.*, 2016, **138**, 13750–13755.
42 B. Chen, J. J. Holstein, S. Horiuchi, W. G. Hiller and G. H. Clever, *J. Am. Chem. Soc.*, 2019, **141**, 8907–8913.
43 B. Chen, J. J. Holstein, A. Platzek, L. Schneider, K. Wu and G. H. Clever, *Chem. Sci.*, 2022, **13**, 1829–1834.
44 J. A. Findlay, K. M. Patil, M. G. Gardiner, H. I. MacDermott-Opeskin, M. L. O'Mara, P. E. Kruger and D. Preston, *Chem.–Asian J.*, 2022, **17**, e202200093.
45 S. Sudan, R. J. Li, S. M. Jansze, A. Platzek, R. Rudolf, G. H. Clever, F. Fadaei-Tirani, R. Scopelliti and K. Severin, *J. Am. Chem. Soc.*, 2021, **143**, 1773–1778.
46 R. J. Li, F. Fadaei-Tirani, R. Scopelliti and K. Severin, *Chem.–Eur. J.*, 2021, **27**, 9439–9445.
47 A. Tarzia, J. E. M. Lewis and K. E. Jelfs, *Angew. Chem., Int. Ed.*, 2021, **60**, 20879–20887.
48 J. E. M. Lewis, *Chem.–Eur. J.*, 2021, **27**, 4454–4460.
49 J. E. M. Lewis, A. Tarzia, A. J. P. White and K. E. Jelfs, *Chem. Sci.*, 2020, **11**, 677–683.
50 S. S. Mishra, S. V. K. Kompella, S. Krishnaswamy, S. Balasubramanian and D. K. Chand, *Inorg. Chem.*, 2020, **59**, 12884–12894.
51 D. Ogata and J. Yuasa, *Angew. Chem., Int. Ed.*, 2019, **58**, 18424–18428.
52 H. Yu, J. Li, C. Shan, T. Lu, X. Jiang, J. Shi, L. Wojtas, H. Zhang and M. Wang, *Angew. Chem., Int. Ed.*, 2021, **60**, 26523–26527.

53 T. Tsutsui, L. Catti, K. Yoza and M. Yoshizawa, *Chem. Sci.*, 2020, **11**, 8145–8150.
54 R.-J. Li, A. Marcus, F. Fadaei-Tirani and K. Severin, *Chem. Commun.*, 2021, **57**, 10023–10026.
55 F. Li and L. F. Lindoy, *Aust. J. Chem.*, 2019, **72**, 731–741.
56 L. Li, D. J. Fanna, N. D. Shepherd, L. F. Lindoy and F. Li, *J. Inclusion Phenom. Macrocyclic Chem.*, 2015, **82**, 3–12.
57 L. S. Lisboa, J. A. Findlay, L. J. Wright, C. G. Hartinger and J. D. Crowley, *Angew. Chem., Int. Ed.*, 2020, **59**, 11101–11107.
58 L. S. Lisboa, D. Preston, C. J. McAdam, L. J. Wright, C. G. Hartinger and J. D. Crowley, *Angew. Chem., Int. Ed.*, 2022, **61**, e202201700.
59 A. J. McConnell, C. S. Wood, P. P. Neelakandan and J. R. Nitschke, *Chem. Rev.*, 2015, **115**, 7729–7793.
60 T. Y. Kim, R. A. S. Vasdev, D. Preston and J. D. Crowley, *Chem.–Eur. J.*, 2018, **24**, 14878–14890.
61 H. Walba and R. W. Isensee, *J. Org. Chem.*, 1961, **26**, 2789–2791.
62 T. M. Krygowski, H. Szatyłowicz and J. E. Zachara, *J. Org. Chem.*, 2005, **70**, 8859–8865.
63 T. R. Chan and V. V. Fokin, *QSAR Comb. Sci.*, 2007, **26**, 1274–1279.
64 T. Zhao, V. M. Lynch and J. L. Sessler, *Org. Biomol. Chem.*, 2022, **20**, 980–983.
65 Y. Qu, X. Du, K. Cheng, Y. Zang, L. Xu, K.-i. Shinohara, M. Teraguchi, T. Kaneko and T. Aoki, *ACS Mater. Lett.*, 2020, **2**, 1121–1128.
66 *SPARTAN'18*, Wavefunction, Inc.
67 We presume that the minor species observed the ^{1}H NMR spectra is a different linkage isomer of $[Pt(\mathbf{L})_4](BF_4)_2$.
68 Repeating the reaction under the same conditions but using CD_3CN as the solvent results in a very similar outcome, with a mixture of products obtained even after seven days (ESI†).
69 J. E. M. Lewis, E. L. Gavey, S. A. Cameron and J. D. Crowley, *Chem. Sci.*, 2012, **3**, 778–784.
70 R. A. S. Vasdev, J. A. Findlay, A. L. Garden and J. D. Crowley, *Chem. Commun.*, 2019, **55**, 7506–7509.
71 V. Marti-Centelles, A. L. Lawrence and P. J. Lusby, *J. Am. Chem. Soc.*, 2018, **140**, 2862–2868.
72 N. Kishi, Z. Li, Y. Sei, M. Akita, K. Yoza, J. S. Siegel and M. Yoshizawa, *Chem.–Eur. J.*, 2013, **19**, 6313–6320.
73 Y.-H. Li, Y. Zhang, Y.-M. Legrand, A. van der Lee, J.-J. Jiang, C.-X. Chen, C.-Y. Su and M. Barboiu, *Dalton Trans.*, 2017, **46**, 15204–15207.
74 D. Ogata and J. Yuasa, *Angew. Chem., Int. Ed.*, 2019, **58**, 18424–18428.
75 H. Yu, J. Li, C. Shan, T. Lu, X. Jiang, J. Shi, L. Wojtas, H. Zhang and M. Wang, *Angew. Chem., Int. Ed.*, 2021, **60**, 26523–26527.
76 J. E. M. Lewis, *Chem.–Eur. J.*, 2021, **27**, 4454–4460.
77 D. P. August, G. S. Nichol and P. J. Lusby, *Angew. Chem., Int. Ed.*, 2016, **55**, 15022–15026.
78 R. A. S. Vasdev, J. A. Findlay, A. L. Garden and J. D. Crowley, *Chem. Commun.*, 2019, **55**, 7506–7509.
79 I. Regeni, B. Chen, M. Frank, A. Baksi, J. J. Holstein and G. H. Clever, *Angew. Chem., Int. Ed.*, 2021, **60**, 5673–5678.
80 R. J. Li, J. Tessarolo, H. Lee and G. H. Clever, *J. Am. Chem. Soc.*, 2021, **143**, 3865–3873.
81 R.-J. Li, J. J. Holstein, W. G. Hiller, J. Andréasson and G. H. Clever, *J. Am. Chem. Soc.*, 2019, **141**, 2097–2103.
82 G. H. Clever, S. Tashiro and M. Shionoya, *Angew. Chem., Int. Ed.*, 2009, **48**, 7010–7012.
83 K. Yazaki, Y. Sei, M. Akita and M. Yoshizawa, *Chem.–Eur. J.*, 2016, **22**, 17557–17561.
84 E. G. Sheetz, Z. Zhang, A. Marogil, M. Che, M. Pink, V. Carta, K. Raghavachari and A. H. Flood, *Chem.–Eur. J.*, 2022, **28**, e202201584.
85 A. Platzek, S. Juber, C. Yurtseven, S. Hasegawa, L. Schneider, C. Drechsler, K. E. Ebbert, R. Rudolf, Q.-Q. Yan, J. J. Holstein, L. V. Schäfer and G. H. Clever, *Angew. Chem., Int. Ed.*, 2022, **61**, e202209305.
86 S. Sudan, F. Fadaei-Tirani, R. Scopelliti, K. E. Ebbert, G. H. Clever and K. Severin, *Angew. Chem., Int. Ed.*, 2022, **61**, e202201823.
87 D. Brynn Hibbert and P. Thordarson, *Chem. Commun.*, 2016, **52**, 12792–12805.
88 P. Thordarson, *Chem. Soc. Rev.*, 2011, **40**, 1305–1323.
89 *BindFit*, **https://supramolecular.org/**.
90 J. E. M. Lewis and J. D. Crowley, *Supramol. Chem.*, 2014, **26**, 173–181.
91 D. Preston, K. M. Patil, A. T. O'Neil, R. A. S. Vasdev, J. A. Kitchen and P. E. Kruger, *Inorg. Chem. Front.*, 2020, **7**, 2990–3001.
92 J. J. Henkelis, J. Fisher, S. L. Warriner and M. J. Hardie, *Chem.–Eur. J.*, 2014, **20**, 4117–4125.
93 L. S. Lisboa, *Synthesis of Heterometallic Supramolecular Cages*, Thesis, Doctor of Philosophy, University of Otago, 2022, Retrieved from **http://hdl.handle.net/10523/12653**.
94 L. S. Lisboa, M. Riisom, H. J. Dunne, D. Preston, S. M. F. Jamieson, L. J. Wright, C. G. Hartinger and J. D. Crowley, *Dalton Trans.*, 2022, **51**, 18438–18445.
95 Y. Fang, J. A. Powell, E. Li, Q. Wang, Z. Perry, A. Kirchon, X. Yang, Z. Xiao, C. Zhu, L. Zhang, F. Huang and H.-C. Zhou, *Chem. Soc. Rev.*, 2019, **48**, 4707–4730.
96 J. Wang, T. A. Young, F. Duarte and P. J. Lusby, *J. Am. Chem. Soc.*, 2020, **142**(41), 17743–17750.
97 A. B. Grommet, M. Feller and R. Klajn, *Nat. Nanotechnol.*, 2020, **15**, 256–271.
98 C. J. Brown, F. D. Toste, R. G. Bergman and K. N. Raymond, *Chem. Rev.*, 2015, **115**, 3012–3035.
99 Y. Xue, X. Hang, J. Ding, B. Li, R. Zhu, H. Pang and Q. Xu, *Coord. Chem. Rev.*, 2021, **430**, 213656.